

Multifunctional Vortex Beam Generation by a Dynamic Reflective Metasurface

Baiyang Liu, Yejun He, Sai-Wai Wong, and Yin Li*

In recent decades, metasurfaces have attracted considerable interest to generate vortex beams, that is, orbital angular momentum (OAM) carrying beams. However, the existing OAM metasurfaces are mostly fixed-mode or with single function. Here a concept of multifunctional vortex beam generation is proposed, and is realized by a dynamic reflective metasurface which is capable of controlling the vortex beam spatiotemporally. The proposed metasurface has the ability to control OAM mode and to observe rotational Doppler effect. As proof of concept, it is presented that the proposed metasurface can generate an $l = -1$ or $l = +1$ OAM mode reconfigurable beam, and an $l = +1$ spinning OAM beam with rotational Doppler effect. Both simulated and measured results show the effectiveness of the proposed multifunctional OAM metasurface which has two different functionalities. The proposed multifunctional OAM metasurface may have potential applications in OAM multiplexing communications and harmonics manipulation by rotational Doppler effect.

manipulation, imaging, detecting spinning object, and both quantum and classical communications.^[4–16]

One property of vortex waves has been recently used is the ability to increase channel capacity by multiplexing multiple beams with different modes through a single aperture, such that each vortex beam has a unique rotational phase front. The OAM multiplexing technology enable different data streams to be transmitted over the same channel. The vortex wave has a rotational phase profile of $\exp(il\theta)$, where θ is the azimuthal angular and l is the unbounded OAM mode which is an integer.^[17] From the phase structure of vortex beam we can see it is associated with the spatial distribution of the EM wave. Vortex beams with different OAM modes l are orthogonal to each other, different data streams can be multiplexed

together and transmitted along the same beam axis. On the OAM receiver side, the transmitted beams are demultiplexed with low crosstalk, hence the channel capacity and spectral efficiency are increased dramatically. OAM multiplexing is of great interest and has been used in optics, terahertz, millimeter-wave and microwave communications.^[18,19] In addition, wireless data are represented by binary sequences, the unlimited OAM modes were proposed and analyzed to encode the wireless data, then decode them by detecting the OAM phase profiles using phase gradient method. Such novel coding scheme may be found potential applications in secure communication systems.^[20,21] Moreover, the unique vortex momentum of OAM beams with a rotational motion can generate a less well-known rotational Doppler effect for EM system.^[5] A similar example of rotational Doppler effect in mechanical system is the watch hand rotate quicker than normal when the watch is rotating at the center. Recently, the rotational Doppler effect of vortex beams was proposed to detect a spinning object and to measure the velocity of fluid flow.^[22–24]


Metamaterials are artificially engineered structures which have been widely used to manipulate the electromagnetic (EM) waves in an unprecedented way. Metasurfaces, as the 2D equivalence of metamaterials are attracted more and more attentions in both science and engineering communities, owing to their ability that can control the amplitude, phase shift, and polarization state of EM waves. Many fascinating applications have been studied by metasurfaces, such as invisibility cloak,^[25,26] negative refraction,^[27,28] radar cross section reduction,^[29,30] etc. The possibility to arbitrarily control

1. Introduction

Angular momentum (AM) of electromagnetic (EM) waves can be decomposed into spin angular momentum (SAM) and orbital angular momentum (OAM).^[1] The well-known SAM is associated with the circular polarization state or intrinsic rotation, and the less well-known OAM is associated with helical phase front or extrinsic rotation. The SAM mode $\sigma = \pm 1$ corresponds to left- and right-hand circular polarization states. The OAM beams are also called vortex beams due to their rotational phase front creating a vortex momentum along the beam axis. In 1935, Beth demonstrated the SAM is able to transfer to a mechanical system.^[2] However, it is until 1990 that vortex beams are being found practical use.^[3] Recently, OAM has been found many applications such as particle

Dr. B. Liu, Prof. Y. He, Prof. S.-W. Wong, Dr. Y. Li
College of Electronics and Information Engineering
Shenzhen University
Shenzhen 518060, China
E-mail: liyinuestc@gmail.com

Dr. B. Liu
State Key Laboratory of Millimeter Waves
Southeast University
Nanjing 211189, China

 The ORCID identification number(s) for the author(s) of this article can be found under <https://doi.org/10.1002/adom.202001689>.

DOI: 10.1002/adom.202001689

EM waves of metasurfaces has been utilized to generate vortex beams in both optics and radio frequency. According to the spatial phase distribution $\exp(il\theta)$ of vortex beam, the metasurfaces can be explicitly designed as OAM generators. Researches have been explored to use transmissive or reflective metasurfaces to generate multiple OAM modes, broadband vortex beams, and reconfigurable OAM mode by active components. Such metasurfaces can generate OAM beams simply and efficiently. However, the existing metasurfaces are mostly fixed-mode or with a single function which are not able to meet the changing demands.^[31–34] In order to meet the needs of different OAM application scenarios, multifunctional OAM generators should be designed.

Owing to new degrees of freedom that spatiotemporal modulation provide, we can manipulate the EM waves' phase not only in space but also in time by a dynamic metasurface.^[35–38] In this paper, we propose a concept to use a dynamic reflective metasurface to realize a multifunctional vortex beam. The proposed OAM metasurface has two different functionalities. On one hand, instead of generating fixed-mode OAM beam, the dynamic OAM metasurface can generate multimode vortex beam that can be used for OAM multiplexing communications. On the other hand, the proposed OAM metasurface can generate a spinning OAM beam through space-time modulation which can be used to observe rotational Doppler effect for harmonics manipulation^[39] or served as a Doppler cloak.^[40] The proposed metasurface has the ability of both OAM mode manipulation and harmonics manipulation, which is thus considered as a multifunctional OAM metasurface. Moreover, a dynamic reflective metasurface working at 10 GHz with $32 \times 32 = 1024$ active unit cells and a 3-bit phase resolution is designed and fabricated. The proposed dynamic metasurface is designed to generate an $l = -1$ or $l = +1$ OAM mode reconfigurable beam and an $l = +1$ spinning OAM beam, these two different functionalities are verified by simulations and experiments, all the results show the proposed metasurface can generate a multifunctional vortex beam efficiently. The proposed multifunctional OAM metasurface concept may pay the novel directions of both metasurfaces and vortex beams.

2. Theoretical Design

A conceptual illustration of the proposed multifunctional vortex beam generation by a metasurface is shown in **Figure 1**. Here a horn feeder emits an incident wave onto the metasurface, and the incident wave is reflected as a multifunctional OAM beam. Each active unit cell with two varactor diodes on the metasurface is a 3-bit phase shifting element. Eight independent time-varying direct current (DC) power supplies U_1-U_8 are used to bias each unit cell then spatiotemporally modulate the reflection phase, therefore changing the operating functionality. Two different functionalities are achieved for the vortex beam reflected by the multifunctional metasurface. Function 1 is to generate an $l = -1$ or $l = +1$ OAM mode reconfigurable beam for OAM multiplexing communications, and Function 2 is to generate an $l = +1$ spinning OAM beam for observation of rotational Doppler effect and harmonics manipulation.

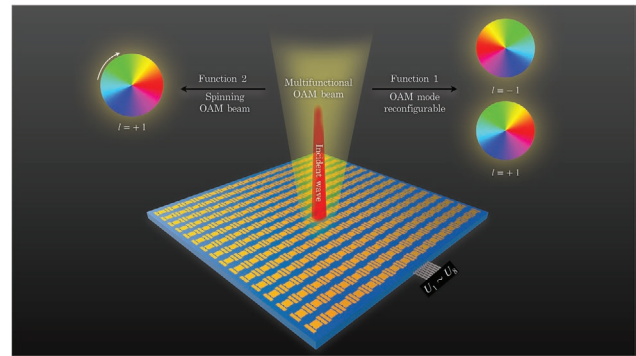


Figure 1. Conceptual illustration of multifunctional vortex beam generation by a metasurface, the metasurface is spatiotemporally modulated by eight independent DC power supplies. The reflected OAM beam has two different functionalities, OAM mode reconfigurable and spinning OAM beam generation, respectively.

3. Unit-Cell Design

Figure 2 shows the 3D illustration of the unit cell of the proposed multifunction OAM metasurface. The unit cell consists of two varactor diodes (MAVR-000120-1411 from MACOM) and three copper layers which are supported by two substrate layers and a thin bonding layer. The equivalent circuit of the varactor diode is shown in **Figure 2**. Here we show the detailed dimensions of the proposed unit cell in **Figure 3**, the central square patch is via to middle copper layer connected to negative “–” electrode, and the rectangle patches on both sides are via to bottom copper layer connected to positive “+” electrode. Two substrate layers are Rogers 4003C with a dielectric constant of 3.55 and a loss tangent of 0.0027, and the bonding layer is Rogers 4450F with a dielectric constant of 3.52 and a loss tangent of 0.004. Note that the unit cell is working at 10 GHz for x-polarization.

Here our unit cell is a 3-bit phase shifting element with a resolution of $\pi/4$. When the bias voltage provides different voltages, the varactor diodes have different capacitances resulting a 3-bit reflection phase, every contiguous state has a phase shifting of $\pi/4$. The simulated reflection amplitude and phase versus varactor capacitance are shown in **Figure 4a–c** shows the simulated bias voltage versus capacitance of varactor diodes and reflection phase, respectively. Simulation is done by the commercial software CST Microwave studio using waveguide

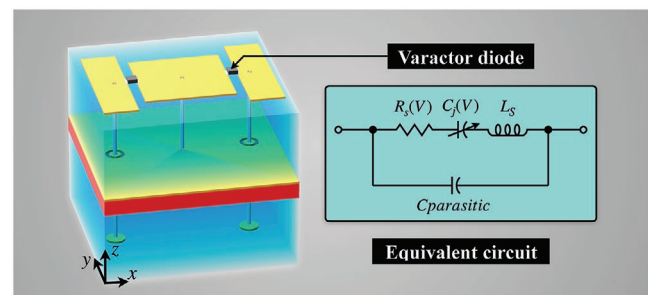


Figure 2. A 3D illustration of the unit-cell structure for multifunctional OAM metasurface, which consists of two varactor diodes for tuning the reflection phase, the equivalent circuit of varactor diode is shown.

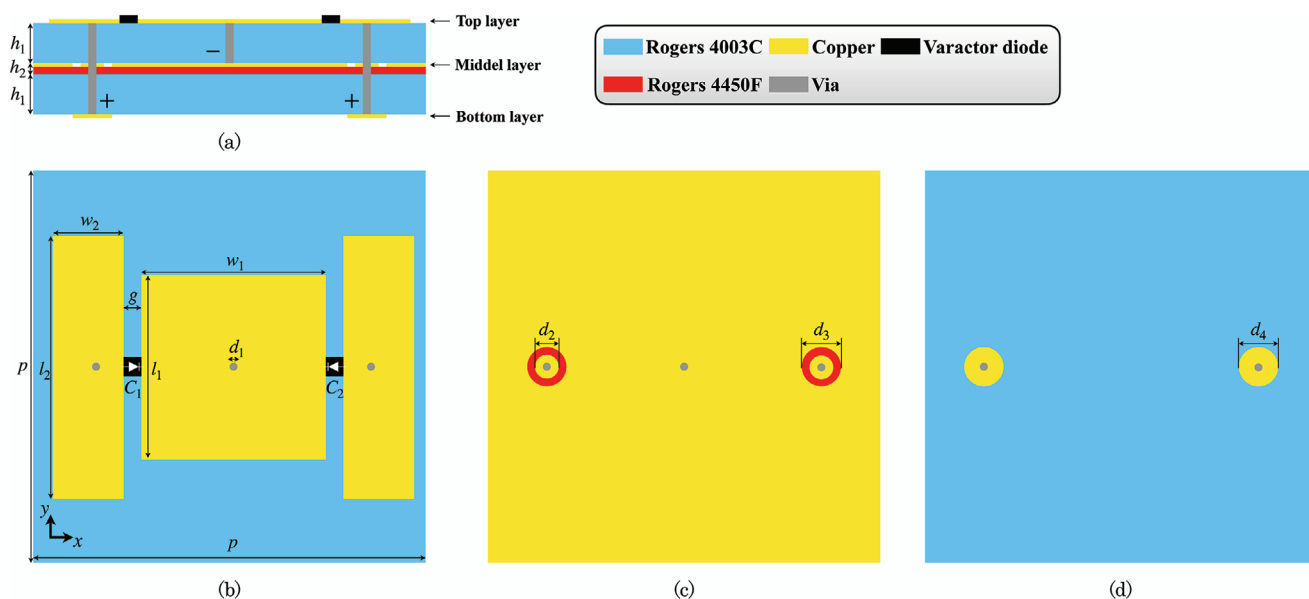


Figure 3. Detailed parameters of the unit cell for multifunctional OAM metasurface. a) Perspective view, electrodes “+” and “-” for two varactor diodes are shown, b–d) are the top view for top layer, middle layer, and bottom layer, respectively. The unit cell is designed at the center frequency of 10 GHz with a spacing of $\lambda/3$. $h_1 = 0.508$ mm, $h_2 = 0.101$ mm, $p = 10$ mm, $w_1 = 4.7$ mm, $w_2 = 1.8$ mm, $l_1 = 4.7$ mm, $l_2 = 6.5$ mm, $g = 0.5$ mm, $d_1 = 0.2$ mm, $d_2 = 0.4$ mm, $d_3 = 0.6$ mm.

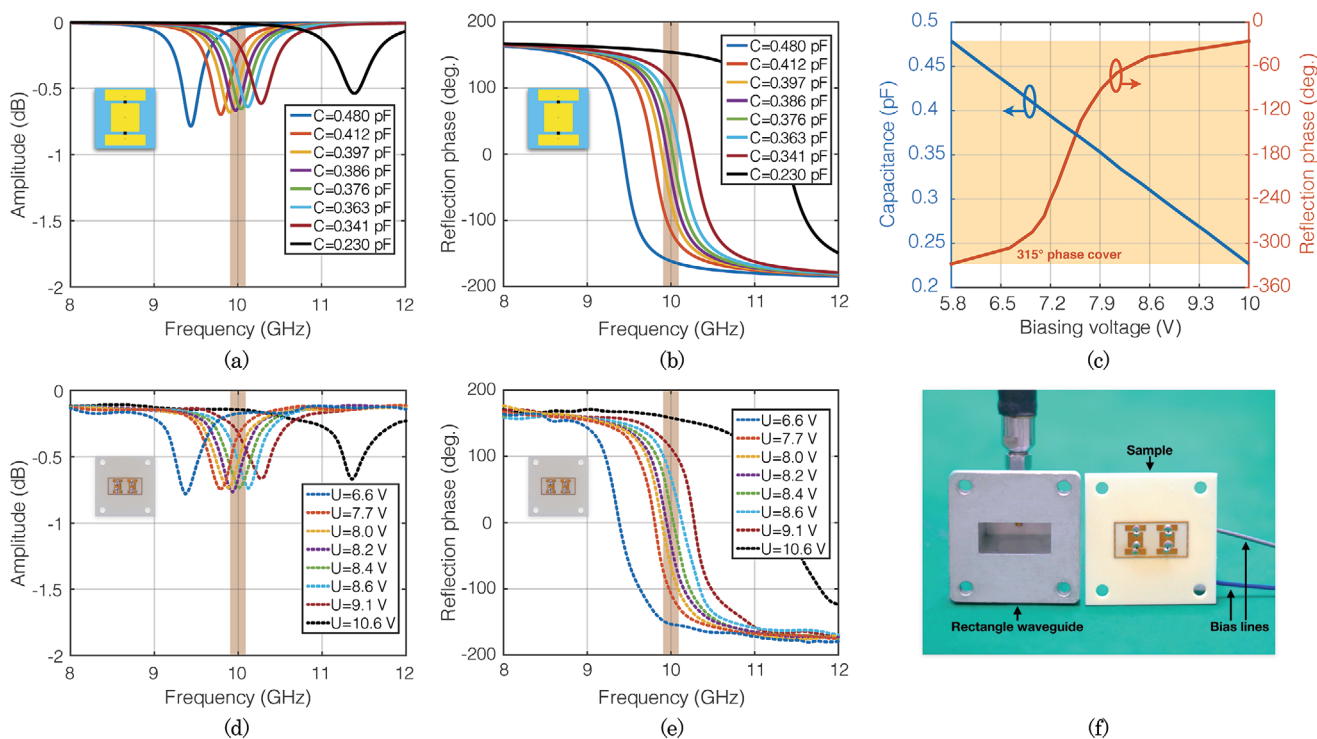


Figure 4. Simulated and measured reflection performances of the unit cell. Simulated a) amplitude and b) reflection phase of the unit cell with different varactor diode capacitances, respectively. c) Red line is simulated reflection phase modulated by bias voltage, blue line is the bias voltage versus varactor diodes capacitance referred by the MAVR-000120-1411 datasheet. The bias voltages we used in the simulation are 5.80, 6.94, 7.19, 7.37, 7.54, 7.76, 8.13, and 10.0 V, respectively. Measured d) amplitude and e) phase of the unit cell with different bias voltages, respectively. f) Measurement setup of reflection coefficient by a rectangle waveguide.

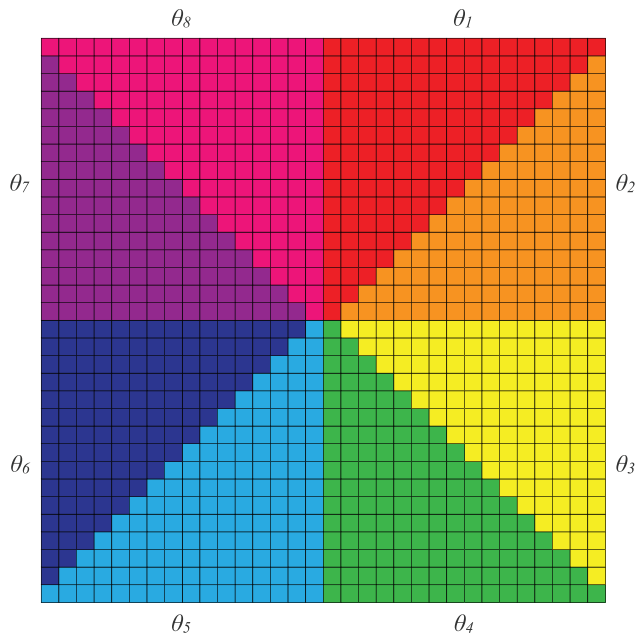


Figure 5. Spatial distribution of the proposed metasurface which consists of eight azimuthal regions θ_1 – θ_8 representing by different colors, 32×32 unit cells are on the metasurface, each region with an independent reflection phase which is biased by an independent DC power supply.

excitation, and the varactor diodes are modeled as the equivalent circuit shown in Figure 2. We can see a 315° phase cover is

obtained, which is used for the 3-bit phase coding. To validate the effectiveness of the unit cell, a sample with two identical unit cells is fabricated, the reflection coefficients of the sample with different bias voltages are measured by a 10 GHz rectangle waveguide. The fixed unit cell in a waveguide is an effective method^[41,42] to obtain the unit cell performance without having too many interferences. The measured reflection amplitudes and phases by different bias voltages are shown in Figures 4d and 4e, respectively. The assembling and measurement setup are shown in Figure 4f. In our measurement, calibration is done by thru-line-reflect method. A good agreement between the simulated and measured results is obtained.

4. Multifunctional OAM Metasurface

As mentioned above, the OAM beam has an azimuthal dependent phase $\phi(\theta) = \phi(x, y) = l \cdot \arctan(x/y)$, where (x, y) is the coordinate on the metasurface plane. In order to simplify the design, we need to discretize the space and reflection phase. There are $32 \times 32 = 1024$ elements on the metasurface, and we split the azimuthal angle into eight different regions θ_1 – θ_8 , each region has a cover range of $\pi/4$, as shown in Figure 5. Eight independent DC power supplies V_1 – V_8 are used to bias the corresponding regions then generating multifunction vortex beam. The bias network for top layer and bottom layer are shown in Figures 6a and 6b, respectively. Hence, the proposed metasurface obtains a three-bit spatial and reflection phase resolution to generate OAM beam, the

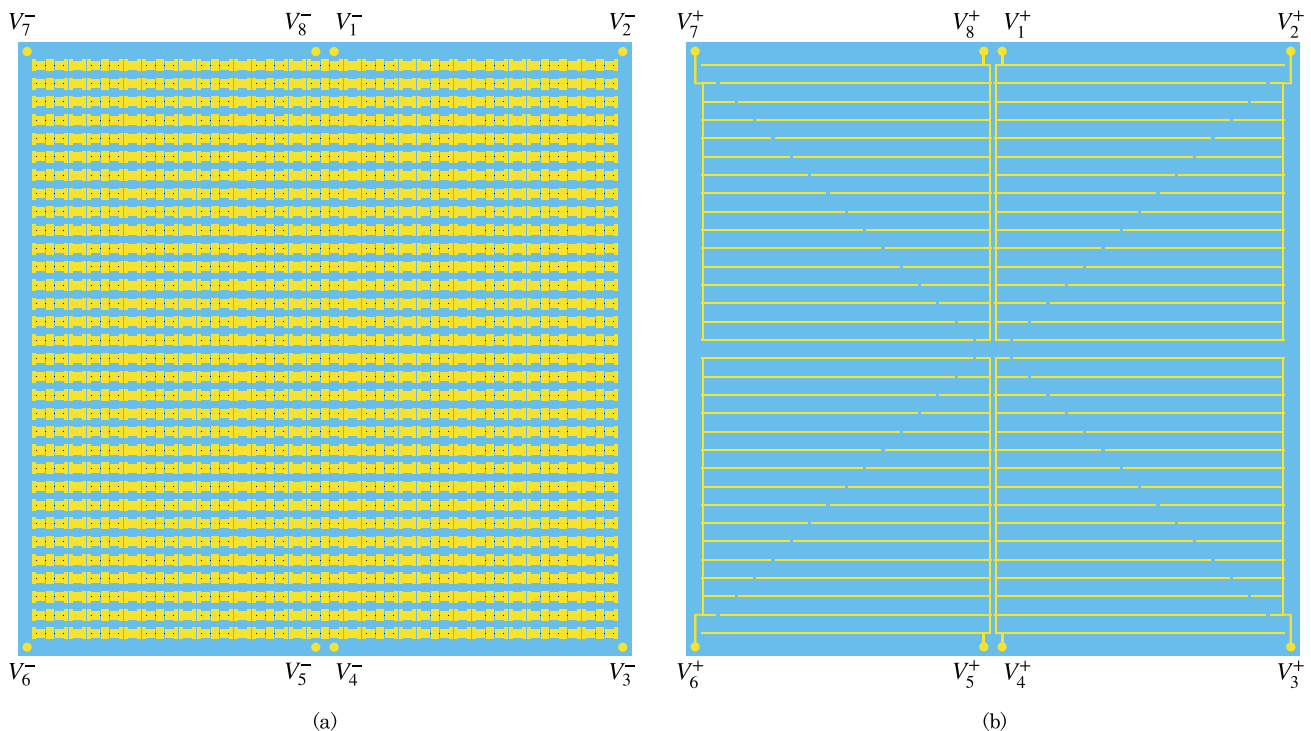


Figure 6. Top view of the overall configuration of the proposed metasurface with 32×32 elements. a) Top layer. b) Bottom layer. Eight independent DC power V_1 – V_8 are used to bias the metasurface. The negative “–” electrodes V_1^- – V_8^- via to the ground are shown on the top layer, and the positive “+” electrodes V_1^+ – V_8^+ with bias lines are shown on the bottom layer.

Phase shifting versus biasing voltage		Phase shifting scheme for OAM mode reconfigurable $\phi(\theta) = l\theta$			Time-varying phase shifting scheme for an $l=+1$ spinning beam $\phi(\theta, t) = l\theta + 2\pi t/T$								
Phase shifting	Biasing voltage		$l = +1$	$l = -1$		$t=0$	$t=1T/8$	$t=2T/8$	$t=3T/8$	$t=4T/8$	$t=5T/8$	$t=6T/8$	$t=7T/8$
0°	6.6 V	θ_1	0°	315°	θ_1	0°	45°	90°	135°	180°	225°	270°	315°
45°	7.7 V	θ_2	45°	270°	θ_2	45°	90°	135°	180°	225°	270°	315°	0°
90°	8.0 V	θ_3	90°	225°	θ_3	90°	135°	180°	225°	270°	315°	0°	45°
135°	8.2 V	θ_4	135°	180°	θ_4	135°	180°	225°	270°	315°	0°	45°	90°
180°	8.4 V	θ_5	180°	135°	θ_5	180°	225°	270°	315°	0°	45°	90°	135°
225°	8.6 V	θ_6	225°	90°	θ_6	225°	270°	315°	0°	45°	90°	135°	180°
270°	9.1 V	θ_7	270°	45°	θ_7	270°	315°	0°	45°	90°	135°	180°	225°
315°	10.6 V	θ_8	315°	0°	θ_8	315°	0°	45°	90°	135°	180°	225°	270°

Figure 7. a) Phase shifting versus bias voltage. b) Phase shifting scheme for the reconfigurable $l = -1$ or $l = +1$ OAM beam generation. c) Phase shifting scheme for an $l = +1$ spinning OAM beam generation.

proposed metasurface can be spatiotemporally modulated by eight time-varying bias voltages. In order to make sure the proposed metasurface has a rotational symmetry structure and simple bias network for observation of rotational Doppler effect, a focusing phase distribution $-2\pi r_{xy}/\lambda$ is not adopted in our design, where r_{xy} is the radial distance from the phase center of horn feeder to the location (x, y) , and λ is operating wavelength.^[34]

In order to generate a multifunctional OAM beam, each azimuthal region has an independent phase shifting. For the OAM mode reconfigurable beam generation, phase shifting is

$$\phi(\theta) = l\theta \quad (1)$$

where $l = -1$ and $l = +1$ are adopted for the proposed metasurface. In addition, for the $l = +1$ spinning OAM beam, a spatiotemporally modulated phase is expressed as follows:^[40]

$$\phi(\theta, t) = l\theta + 2\pi t/T \quad (2)$$

where t is the time variable, T is the period of rotation, symbol minus “+” in the equation means spinning counterclockwise. And the EM wave is

$$E(\theta, t) = A(x, y) \exp(j2\pi f_0 t) \exp(j\phi(\theta, t)) \quad (3)$$

where $A(x, y)$ is the OAM beam doughnut shape amplitude, and f_0 is the initial operating frequency. According to Equations (1) and (2), **Figures 7b** and **7c** show the phase shifting schemes for OAM mode reconfigurable and spinning OAM beam, respectively. Here we set the initial phase shifting 0° is the situation of when capacitance is $C = 0.480$ pF and bias voltage is 6.6 V, as shown in **Figure 7a**, where each phase shifting is mapped to a corresponding bias voltage. In particular, for the spinning OAM beam generation, the proposed metasurface is biased by eight time-varying voltages with a period of T , phase shiftings at eight different time frames are illustrated in **Figure 7c**.

According to the phase shifting schemes in **Figure 7b,c**, we use the commercial software CST Microwave studio to simulate the proposed metasurface with two different functionalities. The

simulation results are shown in **Figure 8** for $l = -1$ or $l = +1$ reconfigurable OAM beam generation, and **Figure 9a** for an $l = +1$ spinning OAM beam generation, respectively. From the simulation results we can see the clear $l = -1$ or $l = +1$ OAM mode reconfiguration and an $l = +1$ spinning OAM beam at eight different time frames. Using Fourier analysis, the spinning OAM beam with rotational Doppler shift can be expressed by:

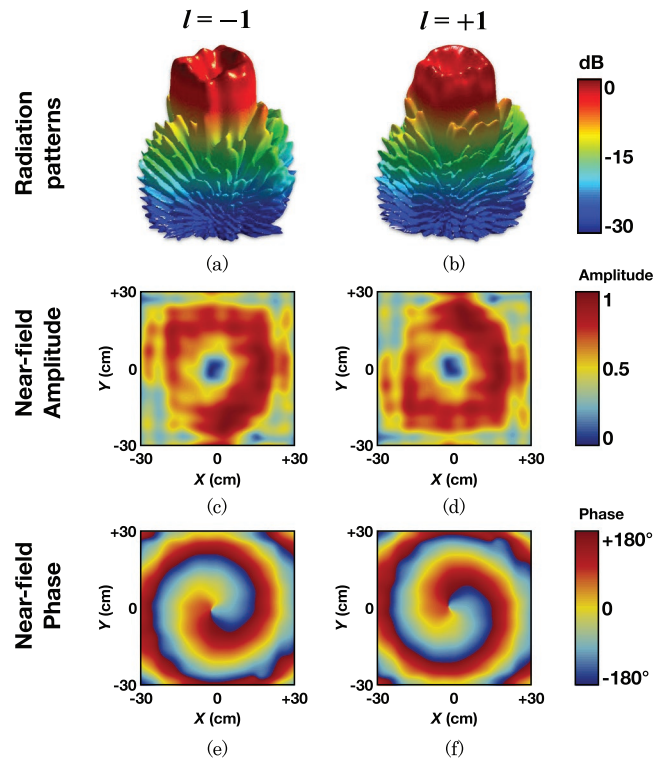


Figure 8. Simulated Function 1: OAM mode reconfigurable. Simulation results for reconfigurable $l = -1$ or $l = +1$ OAM beam generation. Here we use the phase shifting scheme for OAM mode reconfigurable. a) Radiation pattern for $l = -1$ OAM beam. b) Radiation pattern for $l = +1$ OAM beam. c) Near-field amplitude for $l = -1$ OAM beam. d) Near-field amplitude for $l = +1$ OAM beam. e) Near-field phase for $l = -1$ OAM beam. f) Near-field phase for $l = +1$ OAM beam.

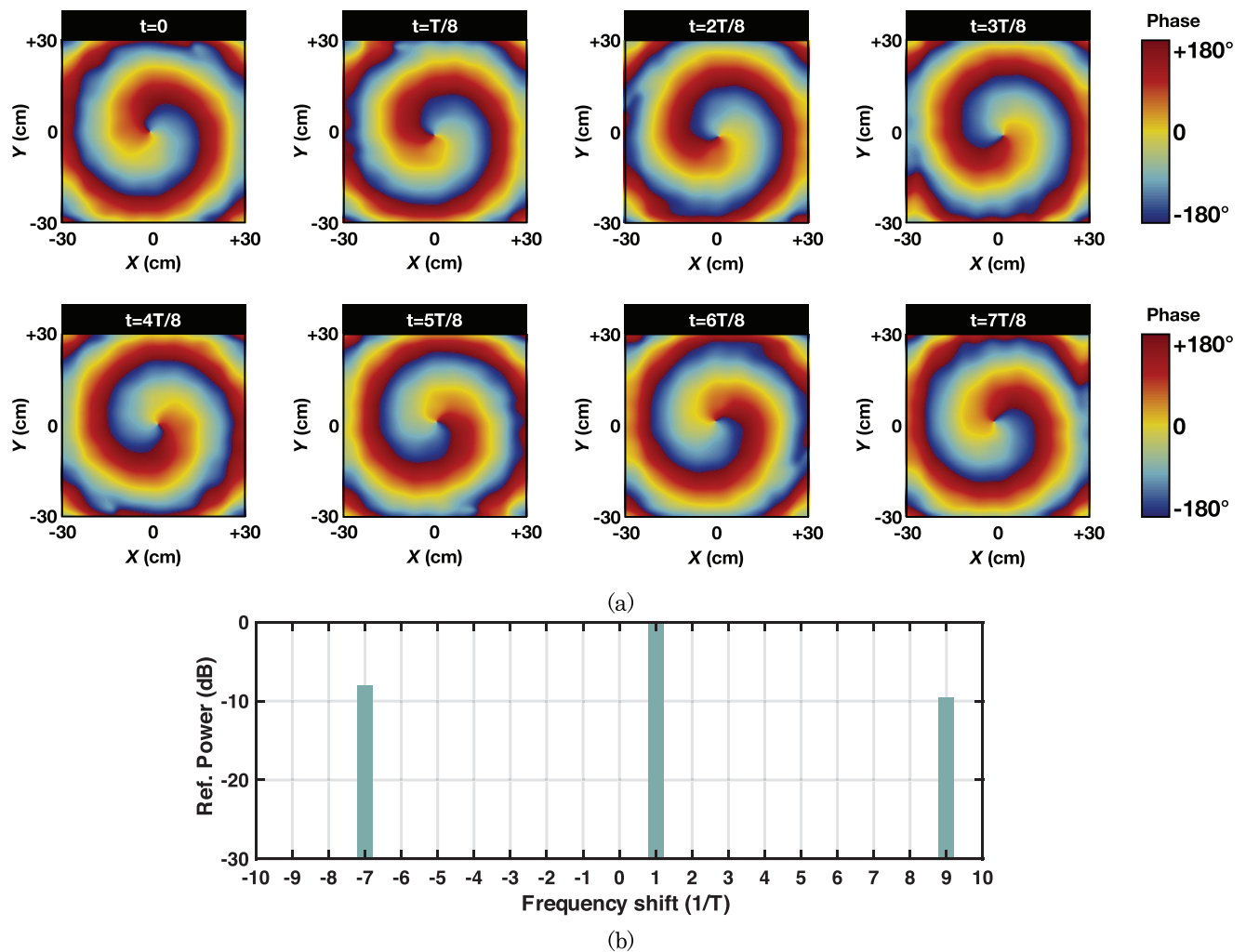


Figure 9. Simulated Function 2: Spinning OAM beam. Here we use the phase shifting scheme for spinning OAM beam. a) Simulation results for an $l = +1$ spinning OAM beam generation. Eight near-field phases corresponding to different time frames. We can see the $l = +1$ OAM beam is spinning with a period T . b) Calculated rotational Doppler shifts for this $l = +1$ spinning OAM beam.

$$E(t) = \sum_{k=-\infty}^{+\infty} a_k \exp\left(jk \frac{2\pi}{T} t\right) \exp(j2\pi f_0 t) \quad (4)$$

where a_k is the harmonic coefficient. The calculated rotational Doppler shifts of the proposed $l = +1$ spinning OAM beam is shown in Figure 9b, a dominant rotational Doppler shift $\Delta f = 1/T$ is observed. Moreover, the low power harmonic frequency shifts are also observed because of the discrete space and reflection phase.

To validate the proposed multifunctional vortex beam generation concept and the effectiveness of the proposed multifunctional OAM metasurface, a prototype of metasurface with $32 \times 32 = 1024$ elements is fabricated. The fabricated metasurface shown in Figure 10 is coated by a color black solder mask, all the varactor diodes on the metasurface are soldered by surface mounting technology. Eight independent DC power supplies are connected to bias network according to the designed phase shifting schemes. The overall view of the prototype in near-field measurement is illustrated in Figure 10. Here we measure the performances of the proposed

metasurface working at Function 1 and Function 2, respectively. The measurement is done in an anechoic chamber, the horn feeder is 300 mm away from the dynamic reflective metasurface, and the planar near-field scanner with an open-ended

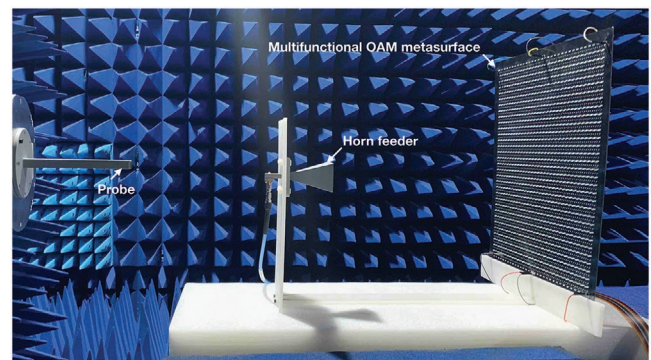


Figure 10. Overall view of the prototype for multifunctional vortex beam generation in the near-field measurement.

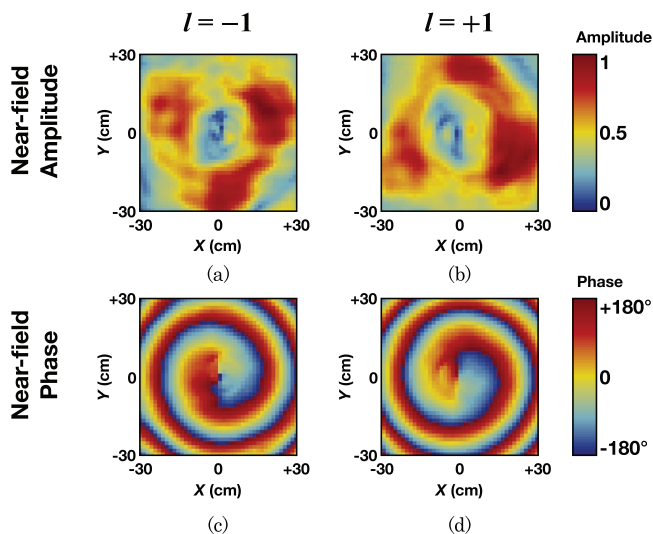


Figure 11. Measured Function 1: OAM mode reconfigurable. Near-field measured results for $l = -1$ or $l = +1$ reconfigurable OAM beam generation. a) Near-field amplitude for $l = -1$ OAM beam. b) Near-field amplitude for $l = +1$ OAM beam. c) Near-field phase for $l = -1$ OAM beam. d) Near-field phase for $l = +1$ OAM beam.

waveguide probe is 500 mm away from the metasurface with an overall scanning range of 300 mm \times 300 mm. The horn feeder is fixed by a polyethylene stand with a dielectric constant of 2.2. Note that the horn feeder is located at the beam null of the reflected beam and the block effect is minimized. Both horn feeder and probe are connected to a network analyzer (Keysight N5224A) to measure the near-field data, the measured results are shown in **Figures 11** and **12** for Function 1 and Function 2, respectively. Each measured near-field pattern consists 40 \times 40 = 1600 electric field data, the scanning resolution is 1.5 cm in both x and y directions, the scanning

time is approximately 20 minutes for each pattern. **Figure 11** is the measured near-field amplitude and phase for an $l = -1$ or $l = +1$ OAM mode reconfigurable beam generation, proving the proposed metasurface can generate reconfigurable OAM beam by control the bias voltages. For the $l = +1$ spinning OAM beam, the spinning pattern is decomposed into eight different static patterns, which are measured individually. **Figure 12** is the measured near-field phases for an $l = +1$ OAM beam at eight different static time frames. It is observed that the OAM beam has a spinning pattern. Moreover, we experimentally demonstrate the rotational Doppler effect by the proposed metasurface. Here we use four arbitrary waveform generators (AWG) which have total eight output channels to provide bias voltages then spin the OAM beam periodically. In this experiment, the open-ended waveguide probe is replaced by a horn receiver which is connected to a spectrum analyzer (Agilent N9020B), and the horn feeder is connected to a signal generator (Agilent N5173B), all the bias voltages are set according to **Figure 7c**, one of the eight bias voltages measured by an oscilloscope is shown in **Figure 13a,c**, the modulation frequencies are $f_1 = 250$ kHz and $f_2 = 500$ kHz, respectively. The other channels have the same waveform but different time delays according to the time-varying phase shifting scheme. **Figure 13b,d** shows the measured spectrum of the reflective signal with different modulation frequencies. The dominant frequency shifts for both cases agree well with the calculated ones. However, the harmonic shifts are not clearly detected due to the fabrication tolerance, synchronization of eight bias voltages and noises at bias voltages. The experiment results clearly show that the proposed metasurface can generate a reflected signal with rotational Doppler shift $\Delta f = 1/T$. However, it is worth noting that the modulation frequency should not exceed the operating bandwidth of the metasurface, this may affect the spectrum due to the signal would be shifted outside the operating frequency.

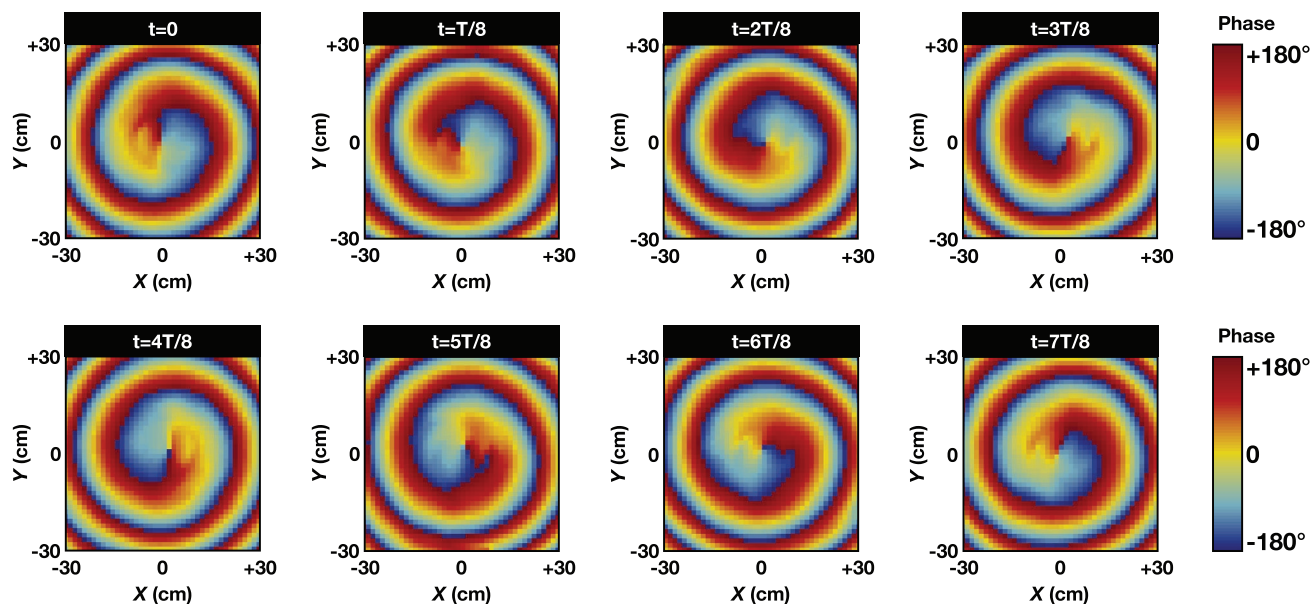


Figure 12. Measured Function 2: Spinning OAM beam. Near-field measured results for an $l = +1$ spinning OAM beam generation. Eight near-field phases corresponding to eight different time frames. We can see the $l = +1$ OAM beam spinning pattern with a period T .

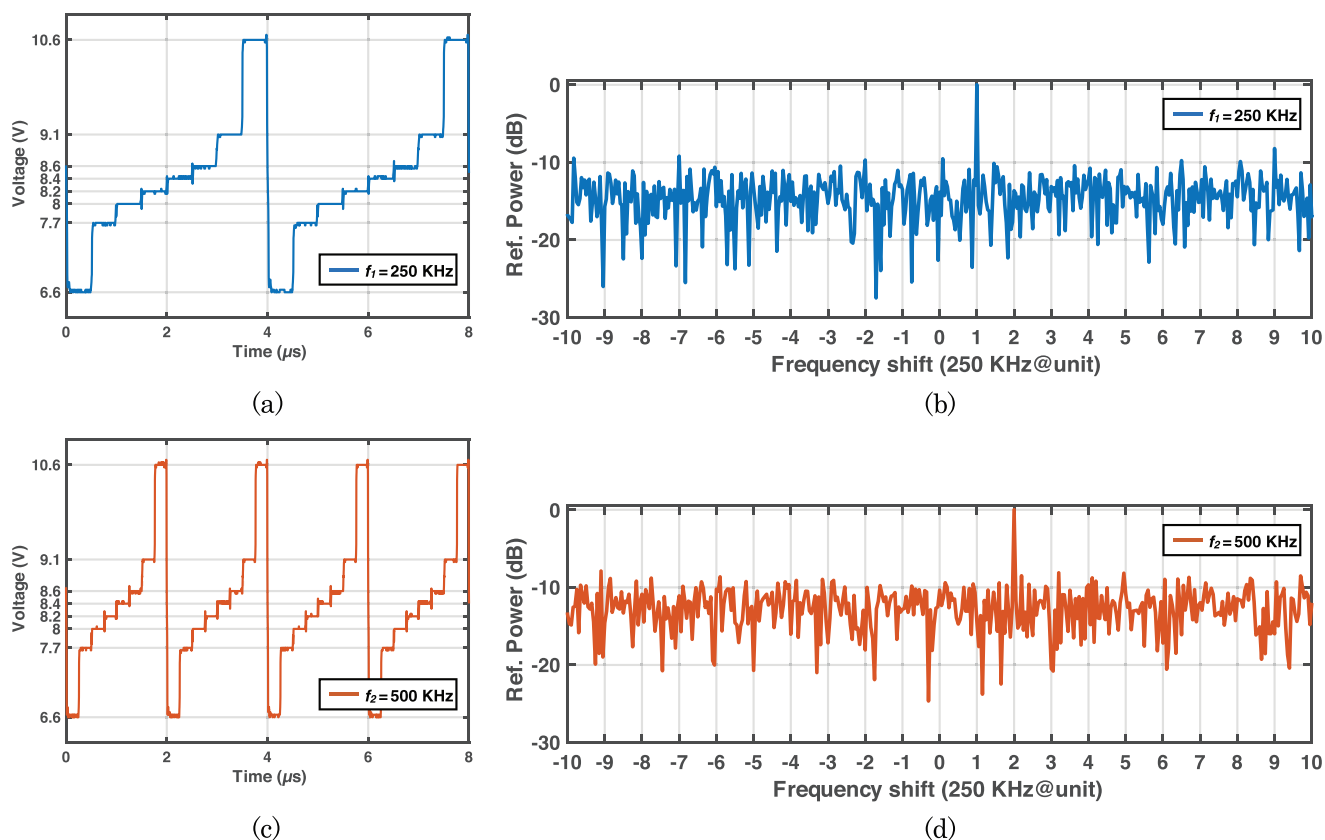


Figure 13. Measured bias voltages and measured spectrum with rotational Doppler shift $\Delta f = 1/T$. a) Bias voltage with modulation frequency $f_1 = 1/T_1 = 250$ kHz and b) is the corresponding measured spectrum. c) Bias voltage with modulation frequency $f_2 = 1/T_2 = 500$ kHz and d) is the corresponding measured spectrum.

5. Conclusion

In summary, to our best knowledge, we first propose the concept of multifunctional vortex beam generation. Such vortex beam has two different functionalities, that is, reconfigurable OAM mode for OAM multiplexing and spinning OAM beam for observation of rotational Doppler effect and harmonics manipulation. Moreover, we use a spatiotemporally modulated reflective metasurface to realize the proposed concept. The simulated and measured results show the effectiveness of the proposed multifunctional vortex beam generation. The proposed dynamic reflective metasurface is different from the fixed-mode or single-function OAM metasurface. Although our work presents the multifunctional OAM beam at radio frequency for 1st order OAM mode, it has no limitation to use this concept for higher frequency and higher order OAM mode. It should be noted that, different from the full space phase tuning metasurfaces, the proposed biasing network in our metasurface can only drive eight independent segments for the purpose of multifunctional OAM beam generation. Future work will focus on generation of multifunctional OAM beam by full space phase tuning programmable metasurface. This work may pave the new directions for dynamic metasurfaces and dynamic OAM beams, and may be found potential applications in wireless communications and radar detection.

Acknowledgements

This work was supported in part by the China Postdoctoral Science Foundation under grant 2020M682876, in part by Guangdong Basic and Applied Basic Research Foundation under grant 2019A151111127, 2019A151111166, in part by State Key Laboratory of Millimeter Waves Foundation under grant K202113, in part by the Shenzhen Science and Technology Programs under grant JCYJ20190808145411289, in part by the Natural Science Foundation of Guangdong Province under grant 2018A030313481, in part by Shenzhen University Research Startup Project of New Staff under grant 860-000002110311, and in part by the Natural Science Foundation of China under grant 62071306 and 61871194.

Conflict of Interest

The authors declare no conflict of interest.

Keywords

metasurfaces, orbital angular momentum, rotational Doppler effect, spatiotemporal modulation

Received: September 29, 2020

Revised: November 17, 2020

Published online:

- [1] A. M. Yao, M. J. Padgett, *Adv. Opt. Photonics* **2011**, 3, 161.
- [2] R. A. Beth, *Phys. Rev.* **1936**, 50, 115.
- [3] L. Allen, M. W. Beijersbergen, R. Spreeuw, J. Woerdman, *Phys. Rev. A* **1992**, 45, 8185.
- [4] A. Belmonte, J. P. Torres, *Opt. Lett.* **2011**, 36, 4437.
- [5] M. P. Lavery, F. C. Speirits, S. M. Barnett, M. J. Padgett, *Science* **2013**, 341, 537.
- [6] L. Marrucci, *Science* **2013**, 341, 464.
- [7] M. P. Lavery, S. M. Barnett, F. C. Speirits, M. J. Padgett, *Optica* **2014**, 1, 1.
- [8] A. Belmonte, C. Rosales-Guzmán, J. P. Torres, *Optica* **2015**, 2, 1002.
- [9] G. Li, T. Zentgraf, S. Zhang, *Nat. Phys.* **2016**, 12, 736.
- [10] S. Franke-Arnold, L. Allen, M. Padgett, *Laser Photonics Rev.* **2008**, 2, 299.
- [11] J. Wang, J.-Y. Yang, I. M. Fazal, N. Ahmed, Y. Yan, H. Huang, Y. Ren, Y. Yue, S. Dolinar, M. Tur, A. E. Winner, *Nat. Photonics* **2012**, 6, 488.
- [12] A. E. Willner, J. Wang, H. Huang, *Science* **2012**, 337, 655.
- [13] J. Wang, *Sci. China: Phys., Mech. Astron.* **2019**, 62, 34201.
- [14] A. Wang, L. Zhu, S. Chen, C. Du, Q. Mo, J. Wang, *Opt. Express* **2016**, 24, 11716.
- [15] J. Wang, *Photonics Res.* **2016**, 4, B14.
- [16] A. E. Willner, H. Huang, Y. Yan, Y. Ren, N. Ahmed, G. Xie, C. Bao, L. Li, Y. Cao, Z. Zhao, J. Wang, *Adv. Opt. Photonics* **2015**, 7, 66.
- [17] S. M. Mohammadi, L. K. Daldorff, J. E. Bergman, R. L. Karlsson, B. Thidé, K. Forozesh, T. D. Carozzi, B. Isham, *IEEE Trans. Antennas Propag.* **2009**, 58, 565.
- [18] Y. Yan, G. Xie, M. P. Lavery, H. Huang, N. Ahmed, C. Bao, Y. Ren, Y. Cao, L. Li, Z. Zhao, A. F. Molisch, M. Tur, M. J. Padgett, A. E. Willner, *Nat. Commun.* **2014**, 5, 8185.
- [19] B. Liu, *Electron. Lett.* **2017**, 53, 1248.
- [20] B. Liu, G. Lin, Y. Cui, R. Li, *Sci. Rep.* **2017**, 7, 9852.
- [21] B. Allen, A. Tennant, Q. Bai, E. Chatziantoniou, *Electron. Lett.* **2014**, 50, 232.
- [22] L. Fang, M. J. Padgett, J. Wang, *Laser Photonics Rev.* **2017**, 11, 1700183.
- [23] O. Korech, U. Steinitz, R. J. Gordon, I. S. Averbukh, Y. Prior, *Nat. Photonics* **2013**, 7, 711.
- [24] S. Barreiro, J. Tabosa, H. Failache, A. Lezama, *Phys. Rev. Lett.* **2006**, 97, 113601.
- [25] H. Chen, B.-I. Wu, B. Zhang, J. A. Kong, *Phys. Rev. Lett.* **2007**, 99, 063903.
- [26] D. Schurig, J. J. Mock, B. Justice, S. A. Cummer, J. B. Pendry, A. F. Starr, D. R. Smith, *Science* **2006**, 314, 977.
- [27] R. A. Shelby, D. Smith, S. Nemat-Nasser, S. Schultz, *Appl. Phys. Lett.* **2001**, 78, 489.
- [28] R. A. Shelby, D. R. Smith, S. Schultz, *Science* **2001**, 292, 77.
- [29] Y. Liu, K. Li, Y. Jia, Y. Hao, S. Gong, Y. J. Guo, *IEEE Trans. Antennas Propag.* **2015**, 64, 326.
- [30] Y. Jia, Y. Liu, Y. J. Guo, K. Li, S.-X. Gong, *IEEE Trans. Antennas Propag.* **2015**, 64, 179.
- [31] S. Yu, L. Li, G. Shi, C. Zhu, X. Zhou, Y. Shi, *Appl. Phys. Lett.* **2016**, 108, 121903.
- [32] C. Ji, J. Song, C. Huang, X. Wu, X. Luo, *Opt. Express* **2019**, 27, 34.
- [33] D. Zhang, X. Cao, H. Yang, J. Gao, X. Zhu, *Opt. Express* **2018**, 26, 24804.
- [34] X. Bai, F. Kong, Y. Sun, G. Wang, J. Qian, X. Li, A. Cao, C. He, X. Liang, R. Jin, W. Zhu, *Adv. Opt. Mater.* **2020**, 8, 2000570.
- [35] L. Zhang, X. Q. Chen, S. Liu, Q. Zhang, J. Zhao, J. Y. Dai, G. D. Bai, X. Wan, Q. Cheng, G. Castaldi, V. Galdi, T. J. Cui, *Nat. Commun.* **2018**, 9, 4334.
- [36] L. Zhang, X. Q. Chen, R. W. Shao, J. Y. Dai, Q. Cheng, G. Castaldi, V. Galdi, T. J. Cui, *Adv. Mater.* **2019**, 31, 1904069.
- [37] L. Li, T. J. Cui, W. Ji, S. Liu, J. Ding, X. Wan, Y. B. Li, M. Jiang, C.-W. Qiu, S. Zhang, *Nat. Commun.* **2017**, 8, 1.
- [38] X. Guo, Y. Ding, Y. Duan, X. Ni, *Light: Sci. Appl.* **2019**, 8, 123.
- [39] J. Y. Dai, J. Zhao, Q. Cheng, T. J. Cui, *Light: Sci. Appl.* **2018**, 7, 1.
- [40] B. Liu, H. Giddens, Y. Li, Y. He, S.-W. Wong, Y. Hao, *Opt. Express* **2020**, 28, 3745.
- [41] A. Clemente, L. Dussopt, R. Sauleau, P. Potier, P. Pouliguen, *IEEE Trans. Antennas Propag.* **2012**, 60, 2260.
- [42] S. Zheng, Y. Yin, J. Fan, X. Yang, B. Li, W. Liu, *IEEE Antennas Wireless Propag. Lett.* **2012**, 11, 240.